Order and Chaos in a 2D potential

8 octobre 2020

1 Background

One of the fundamental question in galactic dynamics is linked to the existence of isolating integral of motion. Isolating integrals are constants along orbits that depend on the coordinates in phase space [1]. They confine the volume of phse space occupied by the orbit. The more an orbit admits integral of motion, the less volume it occupies in phase space.

The classical mean of studying the existence of integral of motion is through the study of orbits in fixed potential, integrating the differential equations of motion and studying the phase space filling of the orbits. This way, one can highlight the presence of phase space regions occupied by orbits of various properties and number of integral of motion. Depending on the potential one can witness the appearance of regular and chaotic zones in the phase space.

This project aims at developing classical techniques for the computation and analysis of orbits and apply them to a know potential, the Hénon-Heiles potential. To compare your results, you will use the associated paper : Hénon M., Heiles C., 1964, AJ, 69, 73.

2 Numerical integration of orbits

2.1 Equation of motion

Before studying the Hénon-Heiles potential, the first step is to develop an orbit integration code. To validate the code, best is to use a simple and well known potential whose properties are fully analytical. For this mean we will use the Kepler potential (point mass)

$$V(R) = -G\frac{m_1 m_2}{R}$$

with G the Gravitation constant, m_1 is the mass of the central body and m_2 the mass of the particle we want to follow the orbit. We can simplify the problem

1. Phase space is the combination of the configuration space (positions x and y) and velocity space (velocities u and v along the x and y axi)s.

assuming $G = m_1 = m_2 = 1$.

The equation of motion are given by Hamilton's equations

$$\begin{cases} \frac{\mathrm{d}\mathbf{q}}{\mathrm{d}t} = \frac{\partial H}{\partial \mathbf{p}} \\ \frac{\mathrm{d}\mathbf{p}}{\mathrm{d}t} = -\frac{\partial H}{\partial \mathbf{q}} \end{cases}$$

with H the Hamiltonian, $\mathbf{p}$ and $\mathbf{q}$ are the configuration space coordinate vector and associated impulsion vector. In our case, we will use the total energy for H.

2.2 Numerical integration

The previous set of equations is a set of differential equations we must integrate to recover the orbit. You will develop three different types of integrator : Euler integrator, Runge-Kutta 2nd order and Runge-Kutta 4th order. These three integrators are numerical integrators for the differential equation

$$\mathbf{w}'(t) = f(t, \mathbf{w}(t))$$

where $\mathbf{w}$ is the coordinate vector in phase space and the prime denotes the time derivative.

Implement the three methods detailed below and compare the their various merits.

Euler method :

Euler methods writes

$$\mathbf{w}_{n+1} = \mathbf{w}_n + h\ f(t, \mathbf{w}_n)$$

where h is a constant integration step and n the step number.

2nd order Runge-Kutta : RK2

RK2 algorithm sums up to this equation

$$\mathbf{w}_{n+1} = \mathbf{w}_n + hf(t + \frac{1}{2}h, \mathbf{w}_{n+1/2})$$

with h the integration step. This method estimates the derivative at half the timestep given by

$$\mathbf{w}_{n+1/2} = \mathbf{w}_n + \frac{1}{2}h\ f(t, \mathbf{w}_n)$$

and

$$\mathbf{w}'_{n+1/2} = f(t + \frac{1}{2}h, \mathbf{w}_{n+1/2})\,.$$

The full integration step requires this estimate and rewrites

$$\mathbf{w}_{n+1} = \mathbf{w}_n + h\mathbf{w}'_{n+1/2}\,.$$

This is an explicit predictor-corrector method.

4th order Runge-Kutta : RK4

RK4 follows the set of equation

$$\mathbf{w}_{n+1} = \mathbf{w}_n + \frac{h}{6}(k_1 + 2k_2 + 2k_3 + k_4)$$
$$\begin{cases} k_1 = f(t_n, \mathbf{w}_n) \\ k_2 = f(t_n + \frac{h}{2}, \mathbf{w}_n + \frac{h}{2}k_1) \\ k_3 = f(t_n + \frac{h}{2}, \mathbf{w}_n + \frac{h}{2}k_2) \\ k_4 = f(t_n + h, \mathbf{w}_n + hk_3)\,. \end{cases}$$

This corresponds to a weighted estimate of the slope of the curve using various lower oder methods.

2.3 Poincaré section

3 Hénon-Heiles potential

For the remaining part of this project, you will use the RK4 method and apply the integrator to the Hénon-Heiles potential given by

$$V(x, y) = \frac{1}{2}(x^2 + y^2 + 2x^2y - \frac{2}{3}y^3)$$

Compute the Poincaré sections [2] for the total energies $E = \frac{1}{100}, \frac{1}{12}, \frac{1}{10}, \frac{1}{8}$ and $\frac{1}{6}$ and compare them to **??**.

4 Chaotic and regular orbits

4.1 Hénon-Heiles technique

The method used by the authors is described in the paper. Implement the method and reproduce the Fig. 7 of the paper.

2. A Poincaré section is the set of points y, v with $x = 0$ and $u > 0$.

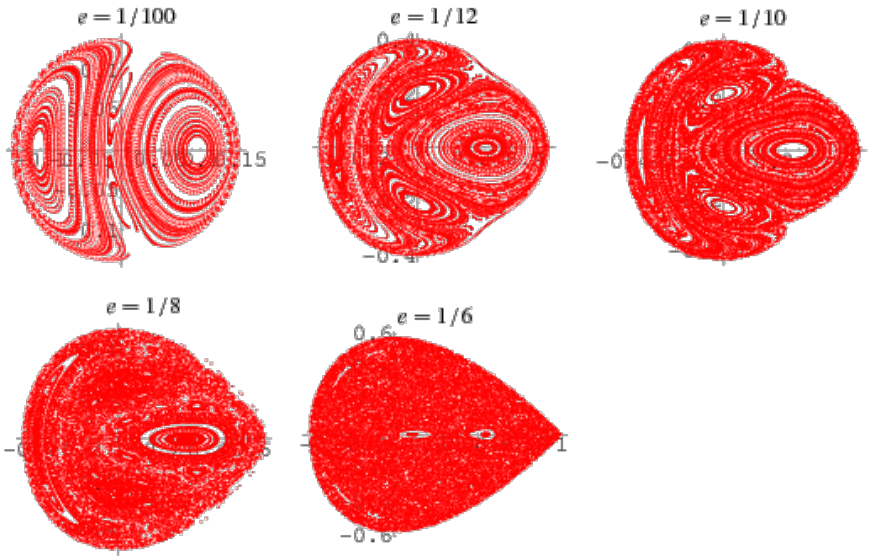

FIGURE 1 – Poincaré sections of the Hénon-Heiles potential for the energy $E = \frac{1}{100}, \frac{1}{12}, \frac{1}{10}, \frac{1}{8}$ and $\frac{1}{6}$.

4.2 Gottwald and Melbourne technique

A more direct way of defining whether an orbit is chaotic or not is proposed in this paper and does not require the computation of two orbits. It is based on the slope of the distance in phase space along an orbit. Implement the method described in the paper (use any coordinate or coordinate combination for this purpose, for example the coordinate x or the velocity u) and compare the result to Fig. 7 of Hénon-Heiles.

THE ASTRONOMICAL JOURNAL VOLUME 69, NUMBER 1 FEBRUARY 1964

The Applicability of the Third Integral Of Motion: Some Numerical Experiments

MICHEL HÉNON* AND CARL HEILES

Princeton University Observatory, Princeton, New Jersey

(Received 7 August 1963)

The problem of the existence of a third isolating integral of motion in an axisymmetric potential is investigated by numerical experiments. It is found that the third integral exists for only a limited range of initial conditions.

1. INTRODUCTION

THERE has recently been a renewal of interest in the question of the existence of the third integral of galactic motion (Contopoulos 1957, 1958, 1960, 1963; Barbanis 1962; van de Hulst 1962, 1963; Ollongren 1962). A thorough review of the problem can be found in Ollongren's work, and we summarize it briefly here. We suppose that the gravitational potential of a galaxy is time-independent and has an axis of symmetry. In a system of cylindrical coordinates R, θ, z, this potential is then a given function $U_g(R, z)$. We are interested in the motion of a star in such a potential. In particular we ask: what part of the 6-dimensional phase space $(R, \theta, z, \dot{R}, \dot{\theta}, \dot{z})$ will be filled by the trajectory of the star if we follow it for a very long time, corresponding to many revolutions within the galaxy?

Since the phase space is six-dimensional, there must exist five independent conservative integrals of the motion; that is, five independent functions

$$I_j(R, \theta, z, \dot{R}, \dot{\theta}, \dot{z}) \qquad (j=1 \text{ to } 5),$$

which are constant along any trajectory. Conversely, a trajectory in phase space is determined by the five equations

$$I_j=C_j \qquad (j=1 \text{ to } 5), \tag{1}$$

where the C_j are five constants. Each equation represents a hypersurface in the phase space, and the trajectory is the intersection of the five hypersurfaces.

But each integral I_j can be isolating or nonisolating (for definition, see Wintner 1947; Lynden-Bell 1962; Ollongren 1962). A nonisolating integral is such that the corresponding hypersurface consists of an infinity of sheets which usually fill the phase space densely, so that for practical purposes the condition $I_j=C_j$ does not give any information and is equivalent to no condition at all. Thus from the physical point of view (as distinct from the mathematical one), nonisolating integrals have no significance. For that reason, isolating integrals are usually called simply "integrals," and the nonisolating integrals are ignored.

In the present case, two isolating integrals are known:

$$I_1=U_g(R,z)+\tfrac{1}{2}(\dot{R}^2+R^2\dot{\theta}^2+\dot{z}^2), \tag{2}$$

$$I_2=R^2\dot{\theta}. \tag{3}$$

They are the total energy and the angular momentum per unit mass of the star around the z axis. It can be shown that two of the other integrals, for example I_4 and I_5, are generally nonisolating. The problem is then: what is the nature of the last integral, I_3?

For many years, it was assumed that I_3 is nonisolating (see, for example, Jeans 1915, 1919; Lindblad 1933; Smart 1938; Van der Pahlen 1947; Lindblad 1959), on the ground that no third integral expressible in analytical form like I_1 and I_2 had been discovered, despite many efforts. But this assumption, as has been often remarked, is in conflict with the observed distribution of stellar velocities near the sun; for it implies that the dispersion of velocities should be the same in the direction of the galactic center and in the direction perpendicular to the galactic plane, whereas the observed dispersions have approximately a 2:1 ratio. More recently, a number of galactic orbits have been computed numerically (Contopoulos 1958, 1963; Ollongren 1962). Quite unexpectedly, all these orbits behaved as if they had not 2, but 3 isolating integrals. As a result, there was some change of opinion on the subject. Attempts were made to prove theoretically the existence of a third integral (see Contopoulos 1963).

In the present paper, we approach the problem again by numerical computations; but, in order to have more freedom of experimentation, we forget momentarily the astronomical origin of the problem and consider it in its general form: does an axisymmetrical potential admit a third isolating integral of motion? Thus, we allow the potential U_g to be an arbitrary function of R and z, not necessarily representing an actual galactic potential.

2. REDUCTION TO A SIMPLER FORM

As is easily seen, if we introduce the function

$$U(R,z)=U_g(R,z)+C_2^2/2R^2, \tag{4}$$

* Present address: Institut d' Astrophysique, Paris.

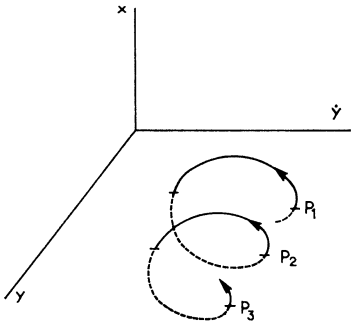

FIG. 1. Definition of the points P_i: $\dot{x}>0$, $x=0$.

where C_2 is the constant value of the angular momentum (3), the equations of motion in R and z become

$$R=-\partial U/\partial R, \qquad z=-\partial U/\partial z. \tag{5}$$

This shows that the problem considered is completely equivalent to the problem of the motion of a particle in a plane in an arbitrary potential U. We shall adopt from now on this new formulation and substitute x and y for R and z. The phase space $(x,y,\dot{x},\dot{y})$ has now four dimensions, and there must exist three independent conservative integrals of the motion. One of them is known and is isolating:

$$I_1=U(x,y)+\tfrac{1}{2}(\dot{x}^2+\dot{y}^2). \tag{6}$$

It is the total energy of the star divided by its mass, as before. There is no integral of angular momentum, because the potential U has no symmetry in general. It can be shown that one of the integrals, say I_3, is generally nonisolating, and the problem is now: what is the nature of the *second* integral I_2?

Because of the existence of the energy integral (6), it is sufficient to know three coordinates of the star in the phase space, such as: x, y, $\dot{y}$; the fourth coordinate $\dot{x}$ can then be obtained from

$$U(x,y)+\tfrac{1}{2}(\dot{x}^2+\dot{y}^2)=E, \tag{7}$$

if we know the energy E. Consequently, we can plot the trajectory in a three-dimensional space $(x,y,\dot{y})$ (see Fig. 1). The value of $\dot{x}^2$ found from (7) should be nonnegative, hence the condition

$$U(x,y)+\tfrac{1}{2}\dot{y}^2\leqslant E \tag{8}$$

which normally defines a bounded volume.

If there is no other isolating integral, the trajectory will fill the volume defined by (8), and we shall call it *ergodic*. If there is a second isolating integral, the trajectory will, instead, lie on a surface, whose equation is found by elimination of $\dot{x}$ between (7) and $I_2=C_2$.

Let us consider the successive intersections of the trajectory with the plane $x=0$, in the upward direction; that is, the successive points P_1, P_2, $\cdots$ of the trajectory which lie in the $(y,\dot{y})$ plane and satisfy

$$x=0, \quad \dot{x}>0. \tag{9}$$

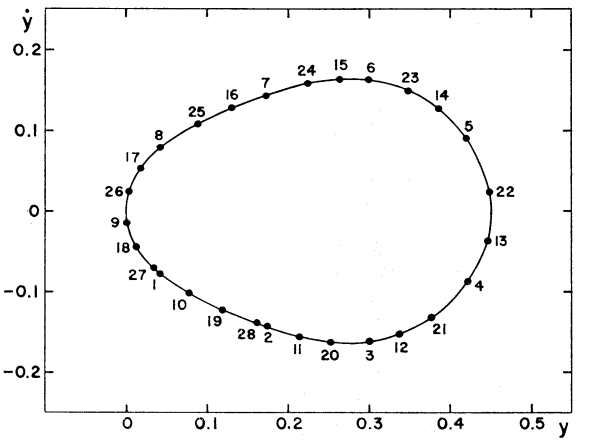

FIG. 3. A typical set of points P_i; $E=0.08333$.

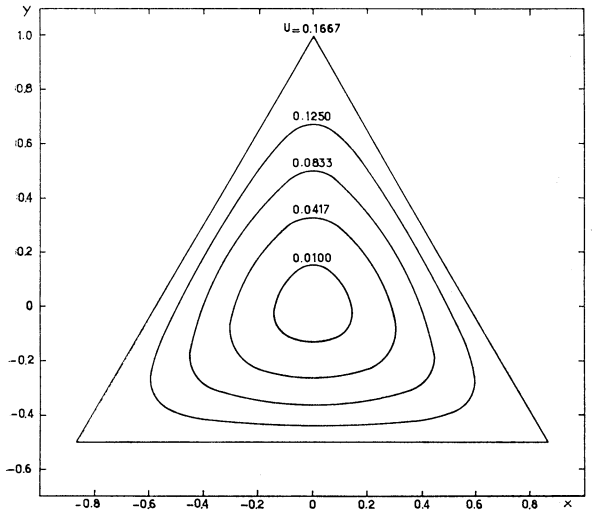

FIG. 2. Equipotential lines of (11).

If we follow the trajectory for an infinite time, there will be in general an infinite sequence of points P_i. If there is no second isolating integral, these points will fill an area, which is the intersection of the volume (8) with the plane $x=0$:

$$U(0,y)+\tfrac{1}{2}\dot{y}^2\leqslant E. \tag{10}$$

But if there is a second isolating integral, the points P_i will lie on a curve. Thus we get a simple criterion for the existence of the second integral: it is sufficient to compute a number of points P_i, plot them in the $(y,\dot{y})$ plane and see whether they lie on a curve or not. This method will be used in what follows.

The passage from a point P_i to the next one P_{i+1} can be considered as a *mapping*. This mapping is completely defined when the potential $U(x,y)$ and the energy E are given. [For, suppose that a point P_i is given. It defines y and $\dot{y}$; x is zero; and $\dot{x}$ is found from (7). Starting from

these four initial values, the trajectory can be integrated to the next point satisfying (9), which is P_{i+1}.] It can also be shown that the mapping is area-preserving [see, e.g., Birkhoff (1927, p. 152); and see Moser (1962) for an important theorem concerning such mappings].

3. RESULTS

After some trials, the following potential was chosen for study:

$$U(x,y)=\tfrac{1}{2}(x^2+y^2+2x^2y-\tfrac{2}{3}y^3) \qquad (11)$$

because: (1) it is analytically simple; this makes the computation of the trajectory easy; (2) at the same time, it is sufficiently complicated to give trajectories which are far from trivial, as will be seen below. It seems probable that the potential (11) is a typical representative of the general case, and that nothing would be fundamentally changed by the addition of higher-order terms.

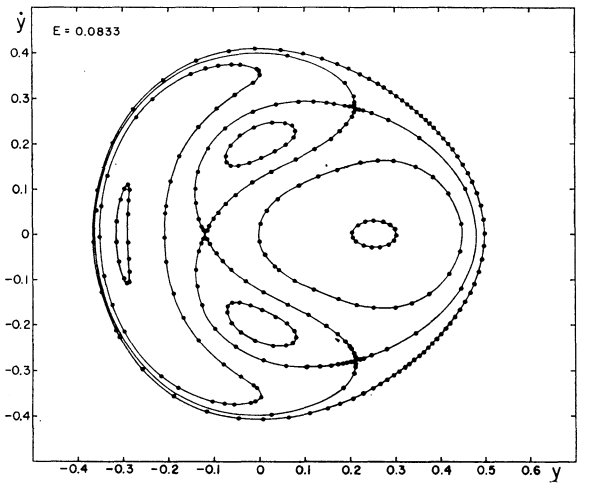

FIG. 4. Results for $E=0.08333$.

Figure 2 shows the equipotential lines. Near the center they tend to be circles; farther out they become elongated in three directions. The particular equipotential $U=\frac{1}{6}$ consists of three straight lines, forming an equilateral triangle.

A number of orbits were computed by numerical integration of the equations of motion:

$$\dot{x}=-\partial U/\partial x=-x-2xy,$$
$$\dot{y}=-\partial U/\partial y=-y-x^2+y^2. \qquad (12)$$

As a check, some of the orbits were computed independently by each of us, using different computers (CDC 1604 and IBM 7090) and different integration schemes (Adams and Runge–Kutta). The following results were obtained using the Runge–Kutta method; during the numerical integration the energy was observed to decrease very slightly ($<|0.00003|$ for 150 orbits).

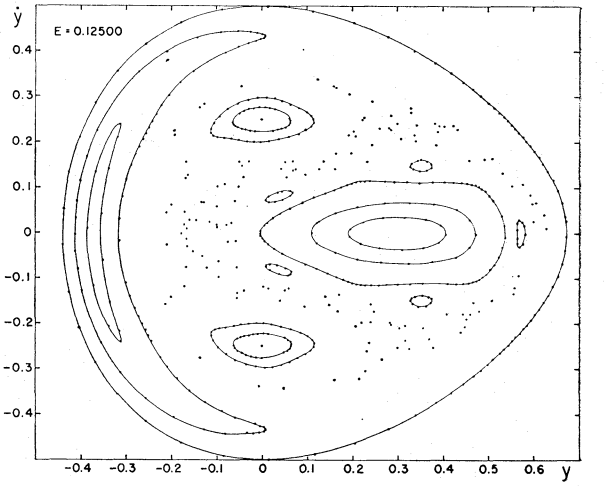

FIG. 5. Results for $E=0.12500$.

Figure 3 shows a set of points P_i for a typical trajectory. They seem to lie exactly on a curve. In fact, more points have been computed than those plotted here; after the 150th point there is still no perceptible deviation from a curve. It may be interesting to remark that the successive points P_1, P_2, $P_3\cdots$ (represented here by 1, 2, $3\cdots$) rotate regularly around the curve. The figure is topologically identical to one where the points P_i would lie on a circle of center O, the angle between OP_i and OP_{i+1} having a constant value α. This constant is not the same for different trajectories. In the case of Fig. 3, its approximate value is $\alpha=0.1143$ (taking one revolution as the unit). α is generally not rational, so that no point P_i will come back exactly on the initial point P_1, and the infinite set of the points P_i is dense everywhere on the curve. If α happens to be a rational number p/q, the point P_{q+1} will be identical with P_1 and the orbit is periodic.

Figure 4 shows the complete picture in the $(y,\dot{y})$ plane, for a given value of the energy: $E=\frac{1}{12}=0.08333$.

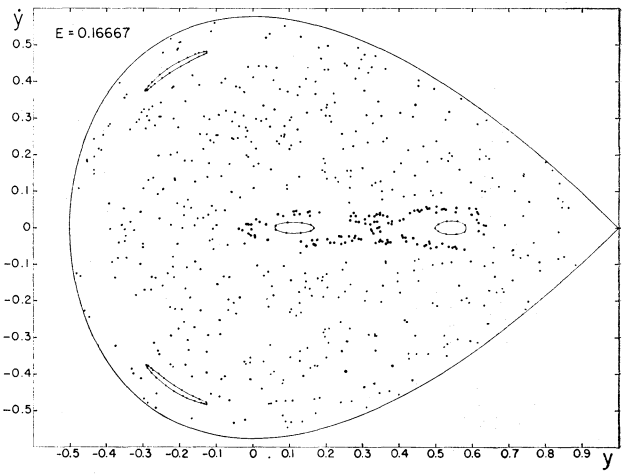

FIG. 6. Results for $E=0.16667$.

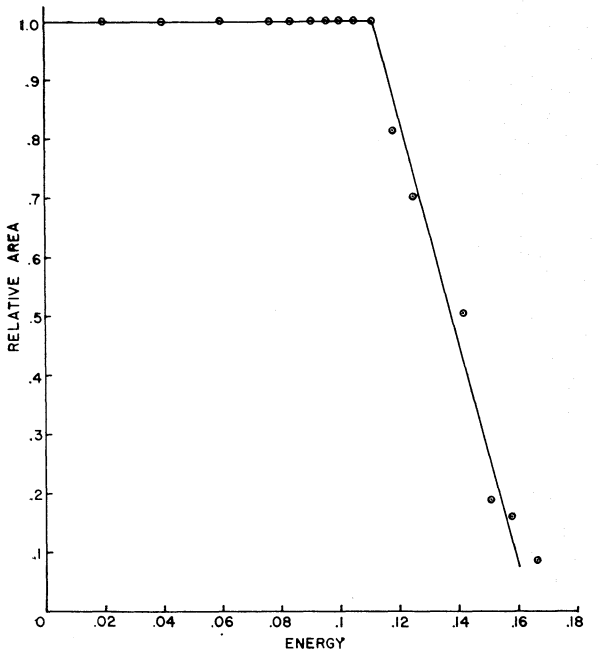

FIG. 7. Relative area covered by the curves as a function of energy, as computed by the method described in the text.

Each set of points linked by a curve corresponds to one computed trajectory. In fact, more trajectories and more points on each have been computed than shown on this picture. It appears that in every case, the points seem to lie exactly on a curve. These curves form a one-parameter family which fills completely the available area, defined by (10). (The boundary of this area is almost identical with the outer curve on Fig. 4.)

In the middle of the four small loops are four invariant points of the mapping (not represented on Fig. 4); they correspond to stable periodic orbits. The three intersections of curves are also invariant points, corresponding to unstable periodic orbits.

This picture seems, like the previous computations by Contopoulos (1958, 1963) and Ollongren (1962), convincing evidence of the existence of a second integral. But here comes the surprise. Figure 5 shows the same picture in the $(y,\dot{y})$ plane for a somewhat higher energy: $E=0.12500$. We still have a set of closed curves around each stable invariant point. But these curves no longer fill the whole area. All the isolated points on Fig. 5 correspond to one and the same trajectory, just as the points on one of the closed curves; but they behave in a completely different way. It is clearly impossible to draw any curve through them. They seem to be distributed at random, in an area left free between the closed curves. Most striking is the fact that this change of behavior seems to occur abruptly across some dividing line in the plane.

The picture is even more complicated than the above description would suggest. For example, the five little loops in the right of the diagram belong to the same trajectory; the successive points P_i jump from one loop to the next. Let us call this feature a *chain of islands*. Other such chains have been found in various parts of the diagram. The number q of the islands in a chain can apparently have any value. As a rule, the dimensions of the islands decrease very rapidly when q increases. Each chain is associated with a stable periodic orbit; the q islands surround the q points which correspond to that orbit. Note that each set of closed curves on Fig. 5 can be considered as a chain constituted by only one island; in both features no ergodic orbit seems to appear. The following properties are also suggested by our results:

(1) there is an infinite number of islands (and of chains);

(2) the set of all the islands is dense everywhere;

(3) but the islands do not cover the whole area since they become very small; there exists a "sea" between the islands and the ergodic trajectory is dense everywhere on the sea.

But, of course, mathematical proofs are needed to establish these points.

Figure 6 shows the situation for a still higher energy: $E=\frac{1}{6}=0.16667$. Again the picture changes drastically. All the isolated points correspond to one trajectory, and it is apparent that this "ergodic" trajectory covers almost the whole area. [The outer line on Fig. 6 is the limit given by (10).] Its random character is most strikingly seen when one plots the successive points; they jump from one part of the diagram to another without any apparent law. Two of the sets of closed curves of Fig. 5, those on the $\dot{y}$ axis, have now disappeared, presumably because their central invariant point has become unstable. The two other sets of closed curves have degenerated, each one into a chain of two small islands, successive points P_i jumping from one to the other. No other chain of islands has been found in Fig. 6; probably they still exist, but the dimensions of the islands are so small that finding them is difficult.

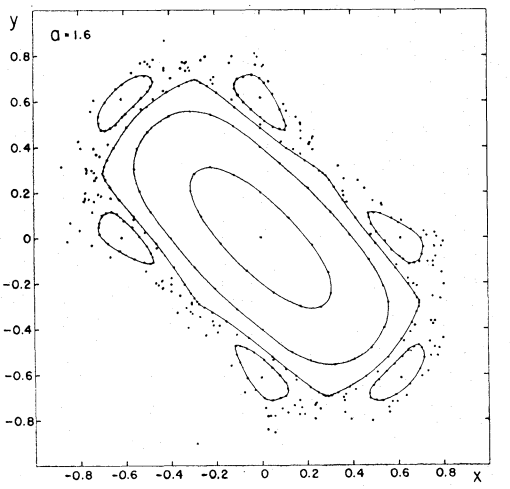

FIG. 8. The iterated mapping (14), for $a=1.6$.

The open circles in the middle of the diagram correspond to a trajectory of a new kind, intermediate between the closed curves and the ergodic behavior. They are approximately situated on an eight-shaped line, but with an important dispersion around it. The ultimate behavior of such an orbit is not known; perhaps the points will always remain in the vicinity of the same line, and fill an eight-shaped band; or perhaps they will after some time penetrate into the ergodic region. Some recent results, not shown here, are in favor of this last hypothesis.

A remarkable feature of Figs. 4 to 6 is the complete change in the picture over a moderate interval of the energy E. For $E=0.08333$, the area is completely covered with curves; for twice that value, the curves are almost completely replaced by an ergodic region. If, instead of the energy, one considers the amplitude of the motion indicated by the equipotential lines of Fig. 2, the change occurs on an even smaller interval.

In order to study this transition in more detail, we have computed, for a number of values of E, the proportion of the total allowable area in the $(y,\dot{y})$ plane which is covered by curves. The following method was used to decide whether a given point P_1 belongs to a curve or to an ergodic orbit. A second initial point P_1' was taken very close to P_1 (usually at a distance 10^{-7}). Then a number (usually 25) of successive transforms of both P_1 and P_1' were computed. Experience had shown previously that if P_1 and P_1' are in a region occupied by curves, the distance P_iP_i' increases only slowly, about linearly, with i; but if P_1 and P_1' are in the ergodic region, the distance P_iP_i' increases rapidly, roughly exponentially. The quantity

$$\mu = \sum_{i=1}^{i=25} (\text{distance } P_iP_i')^2 \qquad (13)$$

was computed, and the point P_1, as well as its transforms, were considered as belonging to the ergodic region if $\mu > \mu_c$, to a curve if $\mu < \mu_c$; μ_c is a chosen constant. The values found for μ covered a very wide range, from about 10^{-12} to 10^{+1}; the criterion seems to be very sensitive, and the exact value chosen for μ_c is not of great importance. Here $\mu_c \cong 10^{-4}$.

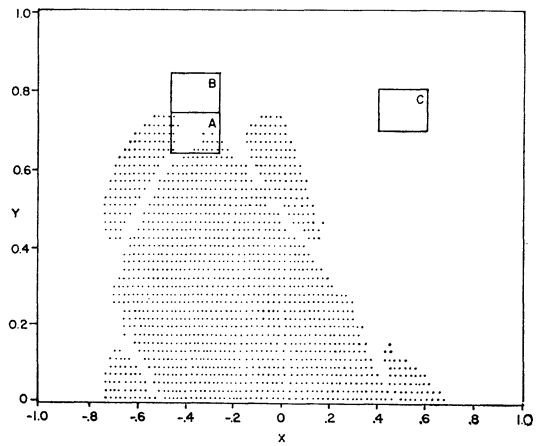

FIG. 9. All nonergodic points in upper half of Fig. 8; Grid size = 0.02.

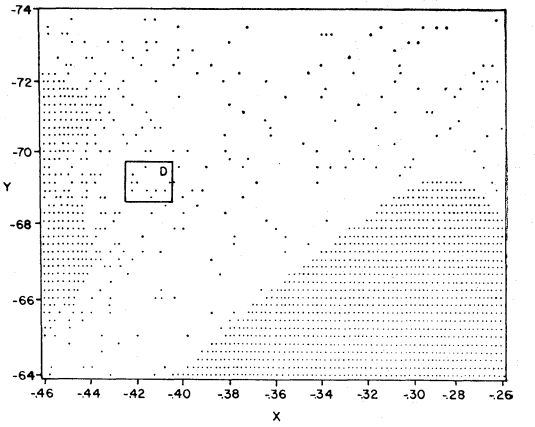

FIG. 10. Enlargement of area A; Grid size = 0.002.

Figure 7 shows the results. Up to a critical energy (about $E=0.11$) the curves cover the whole area; there is no ergodic orbit. For higher energies the area covered by curves shrinks very rapidly. Thus the situation could be very roughly described by saying that the second integral exists for orbits below a "critical energy," and does not exist for orbits above that energy.

$E=\frac{1}{6}$ is the *energy of escape* in the potential (11); for $E>\frac{1}{6}$, the equipotential lines open and the star can eventually escape to infinity, if the orbit is ergodic. The area in the $(y,\dot{y})$ plane becomes infinite and the relative area represented on Fig. 7 ceases to have meaning. No obvious connection exists between the critical energy and the energy of escape; in the present case the critical energy is less than the energy of escape. But results from computations with $U=\frac{1}{2}(x^2+y^2-x^2y^2)$, not shown here, indicate the opposite situation, as do the results of computations by Ollongren (1962) with an approximation to the Galactic potential. However, such a potential, derived from an actual three-dimensional potential, is dependent on the angular momentum assumed; so that more computations for other values of the angular momentum and higher energies are needed to establish the prevalence of the third integral in the Galaxy.

4. STUDY OF A MAPPING

It has been remarked above that the whole problem can be reduced to the study of a plane mapping. As was suggested to us by Dr. Kruskal, one can then define an area-preserving mapping and study it directly, thus by-passing the lengthy integration of orbits. The advantage of this method is that the computation is much simpler and much faster (by a factor 1000 approximately), so that more examples and more points can be computed. The disadvantage is that we are now quite

far from the initial astronomical problem. Also, it is not obvious that an arbitrary area-preserving mapping corresponds to a possible dynamical situation. For these reasons, we give only a short account of the experiments made. The following mapping was studied:

$$X_{i+1}=X_i+a(Y_i-Y_i^3),$$
$$Y_{i+1}=Y_i-a(X_{i+1}-X_{i+1}^3), \qquad (14)$$

where a is a constant. The coordinates of P_i are named here X_i and Y_i.

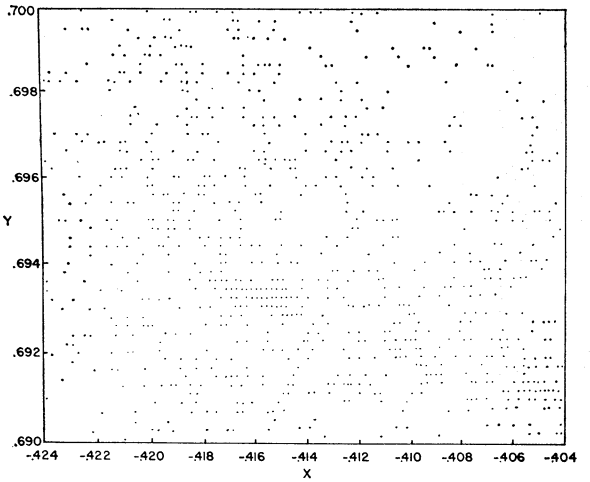

FIG. 11. Enlargement of area D; Grid size=0.0002.

Figure 8 shows the results for $a=1.6$. Each set of points linked by a curve is the set of the successive transforms of an initial point P_1 under the iterated mapping (14). The isolated points are also the successive transforms of a single initial point. The picture is quite similar to the right part of Fig. 5. There is a central region occupied by a set of simple closed curves which surround the stable invariant point $X=Y=0$; a chain of six islands (instead of five); and an outer "ergodic" region. Other chains of islands have been found here too. This similarity suggests that the problem of the area-preserving mapping is really identical with the dynamical problem of the third integral.

Up to 10^5 points have been computed for some of the curves, without any detectable deviation.

Figure 9 represents the upper half of Fig. 8, and Figs. 9–12 were produced in the following manner: initial points were chosen on a grid size indicated in the figure, throughout the whole area of the figure, and 1000 successive iterations of each initial point were computed. Experience has shown that iterations of points which produce an "ergodic orbit" are eventually mapped to infinity; furthermore, this divergence is quite rapid, due to the cubic terms in (14). Thus in Fig. 9 for example, if all 1000 points remained in the vicinity of the origin (this being practically expressed by $X^2+Y^2<100$) the position of the initial point was marked with a dot; otherwise, the position was left blank. The result is a replica of Fig. 8, the only difference being that Fig. 9 shows, to the scale of the grid, *all* initial points whose successive iterations lie on closed curves. Note that it is somewhat distorted, because the vertical and horizontal scales are not equal.

In order to investigate the mapping on a finer scale, we subdivide Fig. 9 into areas A, B, and C. Area A, ten times enlarged, is shown in Fig. 10. The most striking feature is the apparition of a multitude of small islands and tiny details, distributed in a random fashion. It can be remarked also that the boundary of the central region seems very sharp, whereas the boundary of the large island (on the left) is rather fuzzy. Area D of Fig. 10 was again enlarged ten times; see Fig. 11. Again a host of new details emerge. It seems very likely that this would go on indefinitely; with more magnification more details would appear, without end. These results support the hypotheses made above, namely, that there is an infinite number of islands and that their set is dense everywhere.

Area B, which is farther from the center, is represented on Fig. 12. The density of the islands is much smaller than in area A. Also a strong density gradient is apparent in the vertical direction. Area C, still farther out, was found to contain no dots at all to a grid size of 0.002 and therefore is not represented. Thus the density

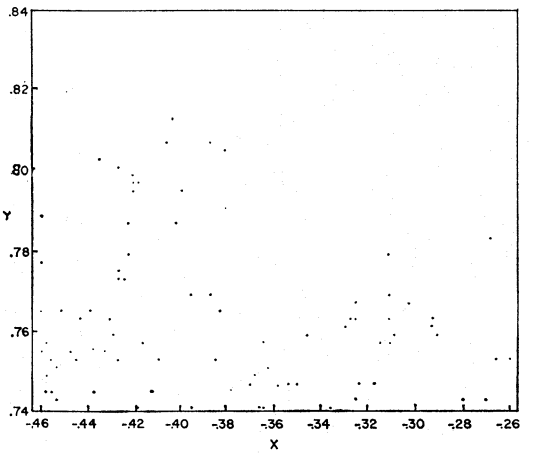

FIG. 12. Enlargement of area B; Grid size=0.002.

of the islands seems to decrease very rapidly as the distance from the central region increases.

5. CONCLUSIONS

We return now to the original three-dimensional problem. The above experiments indicate that the behavior of the orbits is in general quite complicated, and there seems to be no hope of a simple general answer, such as: (a) the third isolating integral always exists; or (b) the third isolating integral does not exist.

The true situation can perhaps be summarized as follows. Consider a given potential, and orbits with given angular momentum and energy. If the energy is small, it seems that a third isolating integral always exists. Perhaps it is only a quasi-integral; but then, to the accuracy of the computers, it is as good as a true integral. If the energy is higher than the critical energy, there are an infinite number of separated regions in the phase space where such a third integral still seems to exist. The space left free between these regions is the "ergodic region" where the third integral is nonisolating. If the energy is further increased, the proportion of allowable phase occupied by this ergodic region increases very rapidly and tends to be the whole space.

A number of questions are raised, for example: are the curves found here exactly or only approximately invariant? What is the topological nature of the set of all the islands? Is it possible to compute the curves directly from the potential, without integrating all the orbits? The ultimate answer to such questions should rest on rigorous mathematical proofs, not on numerical experiments; but the mathematical approach to the problem does not seem too easy.

Finally, it should be mentioned that the problem considered here belongs to the general family of the dynamical systems with two degrees of freedom, and thus is a close relative of the famous restricted three-body problem. Although we cannot attempt it here, a comparison of the two problems would certainly be most fruitful.

ACKNOWLEDGMENTS

Our thanks go to Drs. G. Contopoulos, H. C. van de Hulst, M. Kruskal, J. Moser, and M. Schwarzschild, for many stimulating discussions. One of us (M. Hénon) wants also to thank Princeton University for a one-year stay, during which this work was done; the other was supported by a William Charles Peyton Fellowship during this year.

REFERENCES

Barbanis, B. 1962, *Z. Astrophys.* **56**, 56.
Birkhoff, G. 1927, *Dynamical Systems* (American Mathematical Society, New York).
Contopoulos, G. 1957, *Stockholms Obs. Ann.* **19**, No. 10.
——. 1958, *ibid.* **20**, No. 5.
——. 1960, *Z. Astrophys.* **49**, 273.
——. 1963, *Astron. J.* **68**, 1.
Jeans, J. H. 1915, *Monthly Notices Roy. Astron. Soc.* **76**, 81.
——. 1919, *Problems of Cosmogony and Stellar Dynamics* (Cambridge University Press, New York), p. 233.
Lindblad, B. 1933, *Handbuch der Astrophysik* (Springer-Verlag, Berlin), Vol. V/2, p. 1038.
——. 1959, *Handbuch der Physik* (Springer-Verlag, Berlin), Vol. **53**, p. 28.
Lynden-Bell, D. 1962, *Monthly Notices Roy. Astron. Soc.* **124**, 1.
Moser, J. 1962, *Nachr. Akad. Wiss. Göotingen, Math. Phys. Kl.*, 1.
Ollongren, A. 1962, *Bull. Astron. Inst. Neth.* **16**, 241.
Smart, W. M. 1938, *Stellar Dynamics* (Cambridge University Press, New York), p. 338.
van de Hulst, H. C. 1962, *Bull. Astron. Inst. Neth.* **16**, 235.
——. 1963 (to be published).
van der Pahlen, E. 1947, *Einführung in die Dynamik von Sternsystemen* (Verlag Birkhäuser, Basel), p. 61.
Wintner, A. 1947, *The Analytical Foundations of Celestial Mechanics* (Princeton University Press, Princeton, New Jersey), p. 96.

10.1098/rspa.2003.1183

THE ROYAL SOCIETY

A new test for chaos in deterministic systems

By Georg A. Gottwald[1] and Ian Melbourne[2]

[1]*School of Mathematics and Statistics, University of Sydney, NSW 2006, Australia* (gottwald@maths.usyd.edu.au)

[2]*Department of Mathematics and Statistics, University of Surrey, Guildford, Surrey GU2 7XH, UK* (i.melbourne@surrey.ac.uk)

Received 17 January 2003; accepted 30 April 2003; published online 8 December 2003

We describe a new test for determining whether a given deterministic dynamical system is chaotic or non-chaotic. In contrast to the usual method of computing the maximal Lyapunov exponent, our method is applied directly to the time-series data and does not require phase-space reconstruction. Moreover, the dimension of the dynamical system and the form of the underlying equations are irrelevant. The input is the time-series data and the output is 0 or 1, depending on whether the dynamics is non-chaotic or chaotic. The test is universally applicable to any deterministic dynamical system, in particular to ordinary and partial differential equations, and to maps.

Our diagnostic is the real valued function

$$p(t) = \int_0^t \phi(\boldsymbol{x}(s)) \cos(\theta(s))\, \mathrm{d}s,$$

where ϕ is an observable on the underlying dynamics $\boldsymbol{x}(t)$ and

$$\theta(t) = ct + \int_0^t \phi(\boldsymbol{x}(s))\, \mathrm{d}s.$$

The constant $c > 0$ is fixed arbitrarily. We define the mean-square displacement $\boldsymbol{M}(t)$ for $p(t)$ and set $K = \lim_{t\to\infty} \log \boldsymbol{M}(t)/\log t$. Using recent developments in ergodic theory, we argue that, typically, $K = 0$, signifying non-chaotic dynamics, or $K = 1$, signifying chaotic dynamics.

Keywords: chaos; deterministic dynamical systems; Lyapunov exponents; mean-square displacement; Euclidean extension

1. Introduction

The usual test of whether a deterministic dynamical system is chaotic or non-chaotic is the calculation of the largest Lyapunov exponent λ. A positive largest Lyapunov exponent indicates chaos: if $\lambda > 0$, then nearby trajectories separate exponentially and if $\lambda < 0$, then nearby trajectories stay close to each other. This approach has been widely used for dynamical systems, whose equations are known (Abarbanel *et al*. 1993; Eckmann *et al*. 1986; Parker & Chua 1989). If the equations are not known or one wishes to examine experimental data, this approach is not directly applicable.

However, Lyapunov exponents may be estimated (Wolf *et al*. 1985; Sano & Sawada 1985; Eckmann *et al*. 1986; Abarbanel *et al*. 1993) by using the embedding theory of Takens (1981) or by approximating the linearization of the evolution operator. Nevertheless, the computation of Lyapunov exponents is greatly facilitated if the underlying equations are known and are low-dimensional.

In this article, we propose a new 0–1 test for chaos, which does not rely on knowing the underlying equations, and for which the dimension of the equations is irrelevant. The input is the time-series data and the output is either a '0' or a '1', depending on whether the dynamics is non-chaotic or chaotic. Since our method is applied directly to the time-series data, the only difference in difficulty between analysing a system of partial differential equations (PDEs) or a low-dimensional system of ordinary differential equations is the effort required to generate sufficient data. (As with all approaches, our method is impracticable if there are extremely long transients or once the dimension of the attractor becomes too large.) With experimental data, there is the additional effect of noise to be taken into consideration. We briefly discuss this important issue at the end of this paper. However, our aim in this paper is to present our findings for the situation of noise-free deterministic data.

2. Description of the 0–1 test for chaos

To describe the new test for chaos, we concentrate on the continuous-time case and denote a solution of the underlying system by $\boldsymbol{x}(t)$. The discrete-time case is handled analogously with obvious modifications. Consider an observable $\phi(\boldsymbol{x})$ of the underlying dynamics. The method is essentially independent of the actual form of ϕ—almost any choice of ϕ will suffice. For example, if $\boldsymbol{x} = (x_1, x_2, \ldots, x_n)$, then $\phi(\boldsymbol{x}) = x_1$ is a possible and simple choice. Choose $c > 0$ arbitrarily and define

$$\left.\begin{aligned} \theta(t) &= ct + \int_0^t \phi(\boldsymbol{x}(s))\,\mathrm{d}s, \\ p(t) &= \int_0^t \phi(\boldsymbol{x}(s))\cos(\theta(s))\,\mathrm{d}s. \end{aligned}\right\} \tag{2.1}$$

(Throughout the examples in §§ 3 and 4 we fix $c = 1.7$ once and for all.) We claim that

(i) $p(t)$ is bounded if the underlying dynamics is non-chaotic; and

(ii) $p(t)$ behaves asymptotically like a Brownian motion if the underlying dynamics is chaotic.

The definition of p in (2.1), which involves only the observable $\phi(\boldsymbol{x})$, highlights the universality of the test. The origin and nature of the data which are fed into the system (2.1) are irrelevant for the test, and so is the dimension of the underlying dynamics.

Later on, we briefly explain the justification behind claims (i) and (ii). For the moment, we suppose that the claims are correct and show how to proceed.

To characterize the growth of the function $p(t)$, defined in (2.1), it is natural to look at the mean-square displacement (MSD) of $p(t)$, defined to be

$$\boldsymbol{M}(t) = \lim_{T\to\infty} \frac{1}{T}\int_0^T (p(t+\tau) - p(\tau))^2\,\mathrm{d}\tau. \tag{2.2}$$

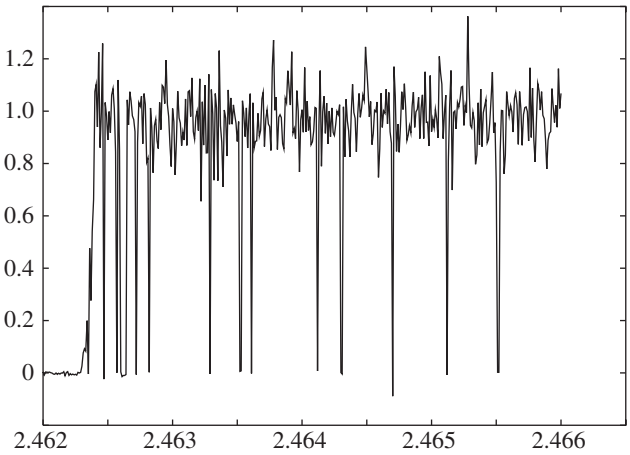

Figure 1. Asymptotic growth rate K of the mean-square displacement (2.2) versus ω for the van der Pol system (3.1) determined by a numerical simulation of the skew-product system (3.1) and (2.1) with $a = d = 5$, $c = 1.7$, $\phi(\boldsymbol{x}) = x_1 + x_2$ and ω varying from 2.462 to 2.466. The integration interval is $T = 2\,000\,000$ after an initial transient of 200 000 units of time.

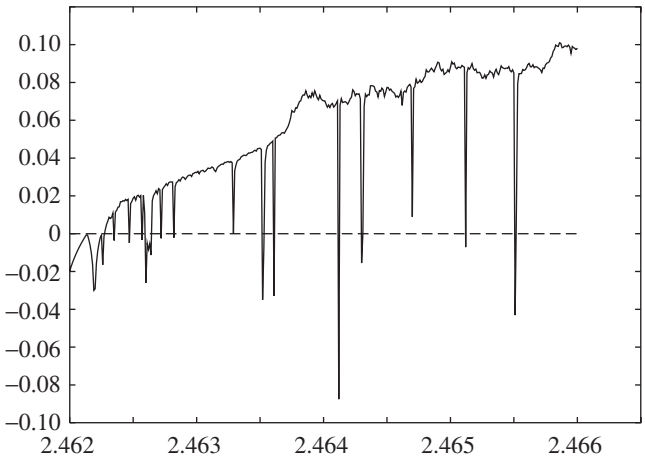

Figure 2. Largest Lyapunov exponent λ versus ω for the van der Pol system (3.1) with $a = d = 5$ and ω varying from 2.462 to 2.466 (cf. Parlitz & Lauterborn 1987). The integration interval is $T = 2\,000\,000$ after an initial transient of 200 000 units of time.

If the behaviour of $p(t)$ is Brownian, i.e. the underlying dynamics is chaotic, then $M(t)$ grows linearly in time; if the behaviour is bounded, i.e. the underlying dynamics is non-chaotic, then $M(t)$ is bounded. We define $K = \lim_{t\to\infty} \log \boldsymbol{M}(t)/\log t$ as the asymptotic growth rate of the MSD. The growth rate K can be numerically determined by means of linear regression of $\log \boldsymbol{M}(t)$ versus $\log t$ (Press *et al.* 1992). (To avoid negative logarithms we actually calculate $\lim_{t\to\infty} \log(\boldsymbol{M}(t) + 1)/\log t$, which obviously does not change the slope K.) This allows for a clear distinction of a non-chaotic and a chaotic system, as K may only take values $K = 0$ or $K = 1$. We have lost the possibility of quantifying the chaos by the magnitude of the largest Lyapunov exponent λ though.

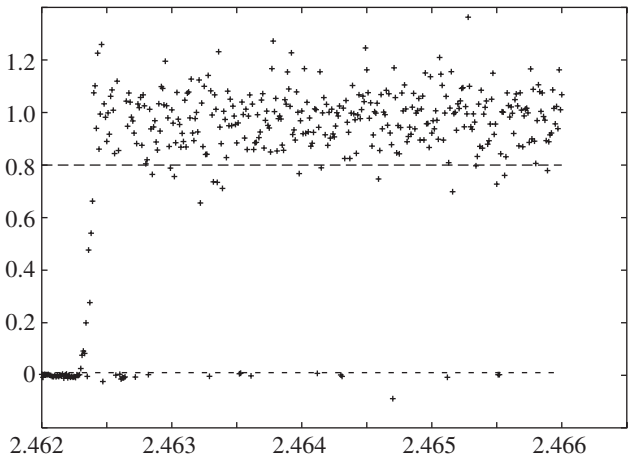

Figure 3. Asymptotic growth rate K versus ω for the van der Pol system (3.1), as in figure 1 with $T = 2\,000\,000$. The horizontal lines represent $K = 0.01$ and $K = 0.8$.

Numerically, one has to make sure that initial transients have died out so that the trajectories are on (or close to) the attractor at time zero, and that the integration time T is long enough to ensure $T \gg t$.

3. An example: the forced van der Pol oscillator

We illustrate the 0–1 test for chaos with the help of a concrete example, the forced van der Pol system,

$$\left.\begin{aligned} \dot{x_1} &= x_2, \\ \dot{x_2} &= -d(x_1^2 - 1)x_2 - x_1 + a\cos\omega t, \end{aligned}\right\} \tag{3.1}$$

which has been widely studied in nonlinear dynamics (van der Pol 1927; Guckenheimer & Holmes 1990). For fixed a and d, the dynamics may be chaotic or non-chaotic depending on the parameter ω. Following Parlitz & Lauterborn (1987), we take $a = d = 5$ and let ω vary from 2.457 to 2.466 in increments of 0.000 01. Choose $\phi(\boldsymbol{x}) = x_1 + x_2$ and $c = 1.7$. We stress that the results are independent of these choices for all practical purposes. As described in § 5, almost all choices will work. (Deliberately poor choices, such as $c = 0$, or $\phi = 7$ or $\phi = t$ obviously fail; sensible choices that fail are virtually impossible to find.)

In figure 1 we show a plot of K versus ω. The periodic windows are clearly seen. As a comparison we show in figure 2 the largest Lyapunov exponent λ versus ω. Since the onset of chaos does not occur until after $\omega = 2.462$, we display the results only for the range $2.462 < \omega < 2.466$ in figures 1 and 2. (Both methods easily indicate regular dynamics for $2.457 < \omega < 2.462$.)

Naturally, we do not obtain the values $K = 0$ and $K = 1$ exactly; the mathematical results that underpin our method predict these values in the limit of infinite integration time. (The same caveat applies equally to the Lyapunov exponent method.) In producing the data for figures 1 and 2, we allowed for a transient of 200 000 units of time and then integrated up to time $T = 2\,000\,000$. In figure 1, data points are connected by straight lines to accentuate the periodic windows. In figure 3, the

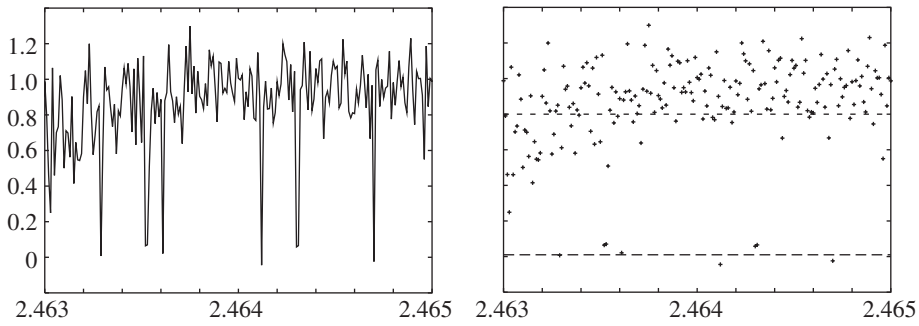

Figure 4. Asymptotic growth rate K versus ω varying from 2.463 to 2.465 for the van der Pol system as in figures 1 and 3 but with integration interval $T = 50\,000$ after an initial transient of 200 000 units of time. The horizontal lines represent $K = 0.01$ and $K = 0.8$.

results are reproduced but without the connecting lines, making it easier to discern the numerically computed values of K. As can be seen in figure 3, for most of the 400 data points in the range of ω, we obtain $K > 0.8$ or $K < 0.01$.

Next, we carry out the 0–1 test for the forced van der Pol system, when there is a more limited quantity of data. The results are shown in figure 4 for $2.463 < \omega < 2.465$. We again allow for a transient time 200 000 but then integrate only for $T = 50\,000$. The transitions between chaotic dynamics and periodic windows are almost as clear with $T = 50\,000$ as they are with $T = 2\,000\,000$ even though the convergence of K to 0 or 1 is better with $T = 2\,000\,000$.

Although it is easy to artificially round off the answer to one of the theoretically predicted possible values of 0 or 1, we have chosen not to do so. Moreover, the closeness of the numerically computed value of K to 0 or 1 provides a natural measure of the reliability of the test.

4. Further examples

To test the method on high-dimensional systems we investigated the driven and damped Kortweg–de Vries (KdV) equation (Kawahara & Toh 1988)

$$u_t + uu_x + \beta u_{xxx} + \alpha u_{xx} + \nu u_{xxxx} = 0 \tag{4.1}$$

on the interval $[0, 40]$ with periodic boundary conditions. This partial differential equation has non-chaotic solutions if the dispersion β is large and exhibits spatio-temporal chaos for sufficiently small β. Note that (4.1) reduces to the KdV equation when $\alpha = \nu = 0$, and reduces to the Kuramoto–Sivashinksy equation when $\beta = 0$.

We fix $\alpha = 2$, $\nu = 0.1$ and vary β. For $\beta = 0$, it is expected that the dynamics of the Kuramoto–Sivashinksy equation is chaotic for these parameter values. As an observable we used $\phi(u(x,t)) = u(x_0,t)$, where x_0 is an arbitrarily fixed position, and we iterated until time $T = 35\,000$. The 0–1 test confirms that the dynamics is chaotic at $\beta = 0$ (with $K = 0.939$). Also, we obtain $K = 0.989$ at $\beta = 0.1$ and $K = 0.034$ at $\beta = 4$, indicating chaotic and regular dynamics, respectively, at these two parameter values.

Finally, for discrete dynamical systems, we tried out the test with an ecological model whose chaotic component is coupled with strong periodicity (Cazelles &

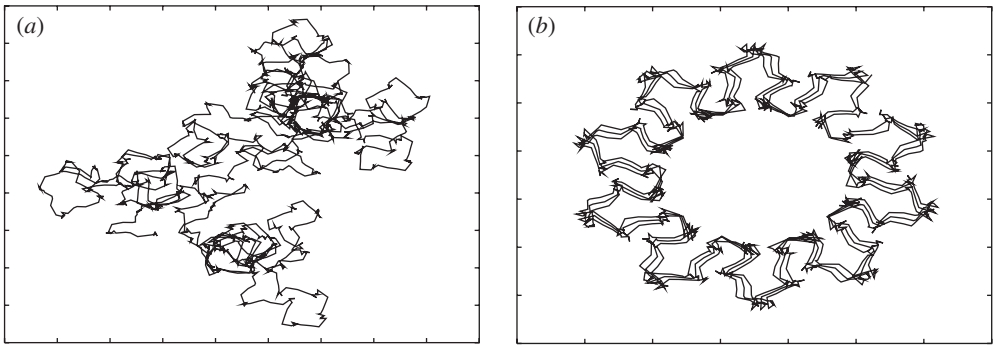

Figure 5. The dynamics of the translation components (p, q) of the $\boldsymbol{E}(2)$-extension (5.1) for the van der Pol system (3.1) with $a = d = 5$, $c = 1.7$, $\phi(\boldsymbol{x}) = x_1 + x_2$. These plots were obtained by integrating for $T \sim 1400$ (with time-step 0.01). (a) An unbounded trajectory is shown corresponding to chaotic dynamics at $\omega = 2.465\,50$. (b) A bounded trajectory is shown corresponding to regular dynamics at $\omega = 2.465\,51$.

Ferriere 1992; Brahona & Poon 1996). The model

$$x_{k+1} = 118 y_k \exp(-0.001(x_k + y_k)),$$
$$y_{k+1} = 0.2 x_k \exp(-0.07(x_k + y_k)) + 0.8 y_k \exp(-0.05(0.5 x_k + y_k))$$

has a non-connected chaotic attractor consisting of seven connected components. Our test yields $K = 1.023$ with only 10 000 data points and clearly shows that the dynamics is chaotic.

5. Justification of the 0–1 test for chaos

The function $p(t)$ can be viewed as a component of the solution to the skew-product system

$$\left.\begin{aligned} \dot{\theta} &= c + \phi(\boldsymbol{x}(t)), \\ \dot{p} &= \phi(\boldsymbol{x}(t)) \cos\theta, \\ \dot{q} &= \phi(\boldsymbol{x}(t)) \sin\theta, \end{aligned}\right\} \tag{5.1}$$

driven by the dynamics of the observable $\phi(\boldsymbol{x}(t))$. Here (θ, p, q) represent coordinates on the Euclidean group $\boldsymbol{E}(2)$ of rotations θ and translations (p, q) in the plane.

We note that inspection of the dynamics of the (p, q)-trajectories of the group extension provides very quickly (for small T) a simple visual test of whether the underlying dynamics is chaotic or non-chaotic, as can be seen from figure 5.

In Nicol *et al*. (2001) it has been shown that, typically, the dynamics on the group extension is sublinear and furthermore that the dynamics is bounded if the underlying dynamics is non-chaotic and unbounded (but sublinear) if the underlying dynamics is chaotic. Moreover, the p and q components each behave like a Brownian motion on the line if the chaotic attractor is uniformly hyperbolic (Field *et al*. 2003). A non-degeneracy result of Nicol *et al*. (2001) ensures that the variance of the Brownian motion is non-zero for almost all choices of observable ϕ. Recent work by Melbourne & Nicol (2003) indicates that these statements remain valid for large classes of non-uniformly hyperbolic systems, such as Hénon-like attractors.

There is a weaker condition on the 'chaoticity' of X that guarantees the desired growth rate $K = 1$ for the mean-square displacement (2.2): namely that the autocorrelation function of $\phi(\boldsymbol{x})\cos(\theta)$ decays at a rate that is better than quadratic. More precisely, let $\boldsymbol{x}(t)$ and $\theta(t)$ denote solutions to the skew-product equations (5.1) with initial conditions $\boldsymbol{x}_0$ and θ_0, respectively. If there are constants $C > 0$ and $\alpha > 2$ such that

$$\left| \int \phi(\boldsymbol{x}(t))\cos(\theta(t))\phi(\boldsymbol{x}_0)\cos\theta_0 \,\mathrm{d}\boldsymbol{x}_0 \,\mathrm{d}\theta_0 \right| \leqslant Ct^{-\alpha},$$

for all $t > 0$, then $K = 1$ as desired (Biktashev & Holden 1998; Ashwin *et al*. 2001; Field *et al*. 2003). (Again, results of Nicol *et al*. (2001), Field *et al*. (2003) and Melbourne & Nicol (2003) ensure that the appropriate non-degeneracy condition holds for almost all choices of ϕ.) There is a vast literature on proving decay of correlations (Baladi 1999) and this has been generalized to the equivariant setting for discrete time by Field *et al*. (2003) and Melbourne & Nicol (2003) and for continuous time by Melbourne & Török (2002). It follows from these references that $K = 1$, for large classes of chaotic dynamical systems.

One might ask why it is not better to work, instead of the $\boldsymbol{E}(2)$-extension, with the simpler $\mathbb{R}$-extension

$$\dot{p} = \phi(\boldsymbol{x}(t)).$$

In principle, $p(t)$ can again be used as a detector for chaos. However, by the ergodic theorem $p(t)$ will typically grow linearly with rate equal to the space average of ϕ. This would lead to $K = 2$ irrespective of whether the dynamics is regular or chaotic. Hence, it is necessary to subtract the linear term of $p(t)$ in order to observe the bounded/diffusive growth that distinguishes between regular/chaotic dynamics. Subtracting this linear term is a highly non-trivial numerical obstruction. The inclusion of the θ variable in the definition (2.1) of $p(t)$ and in the skew product (5.1) kills off the linear term.

6. Discussion

We have established a simple, inexpensive and novel 0–1 test for chaos in deterministic systems. (It is not the purpose of this paper to study stochastic systems.) The computational effort is of low cost, both in terms of programming efforts and in terms of actual computation time. The test is a binary test in the sense that it can only distinguish between non-chaotic and chaotic dynamics. This distinction is extremely clear by means of the diagnostic variable K, which has values either close to 0 or close to 1. The most powerful aspect of our method is that it is independent of the nature of the vector field (or data) under consideration. In particular the equations of the underlying dynamical system do not need to be known, and there is no practical restriction on the dimension of the underlying vector field. In addition, our method applies to the observable $\phi(\boldsymbol{x}(t))$ rather than the full trajectory $\boldsymbol{x}(t)$.

Related ideas (though not with the aim of detecting chaos) have been used for PDEs in the context of demonstrating hypermeander of spirals in excitable media (Biktashev & Holden 1998), where the spiral tip appears to undergo a planar Brownian motion (see also Ashwin *et al*. 2001). We note also the work of Coullet & Emilsson (1996), who studied the dynamics of Ising walls on a line, where the motion is the superposition of a linear drift and Brownian motion. (This is an example of an

$\mathbb{R}$-extension, which we mentioned briefly in § 5. As we pointed out then, the linear drift is an obstruction to using an $\mathbb{R}$-extension to detect chaos.)

From a purely computational point of view, the method presented here has a number of advantages over the conventional methods using Lyapunov exponents. At a more technical level, we note that the computation of Lyapunov exponents can be thought of abstractly as the study of the $\boldsymbol{GL}(n)$-extension

$$\dot{\boldsymbol{A}} = (d\boldsymbol{f})_{\boldsymbol{x}(t)}\boldsymbol{A},$$

where $\boldsymbol{GL}(n)$ is the space of $n \times n$ matrices, $\boldsymbol{A} \in \boldsymbol{GL}(n)$ and n is the size of the system. Note that the extension involves n^2 additional equations and is defined using the linearization of the dynamical system. To compute the dominant exponent, it is still necessary to add n additional equations, again governed by the linearized system. In contrast, our method requires the addition of two equations.

In this paper, we have concentrated primarily on the idealized situation, where there is an, in principle, unlimited amount of noise-free data. However, in § 3 we also demonstrated the effectiveness of our method for limited datasets. An issue which will be pursued in further work is the effect of noise, which is inevitably present in all experimental time-series. Preliminary results show that our test can cope with small amounts of noise without difficulty. A careful study of this capability, and comparison with other methods, is presently in progress.

We are grateful to Philip Aston, Charlie Macaskill and Trevor Sweeting for helpful discussions and suggestions. The research of G.G. was supported in part by the European Commission funding for the Research Training Network 'Mechanics and Symmetry in Europe' (MASIE). The research of G.G. and I.M. was supported in part by EPSRC grant GR/S22714/01.

References

Abarbanel, H. D. I., Brown, R., Sidorovich, J. J. & Tsimring, L. S. 1993 The analysis of observed chaotic data in physical systems. *Rev. Mod. Phys.* **65**, 1331–1392.

Ashwin, P., Melbourne, I. & Nicol, M. 2001 Hypermeander of spirals: local bifurcations and statistical properties. *Physica* D **14**, 275–300.

Baladi, V. 1999 Decay of correlations. In *Smooth ergodic theory and its applications, Proc. Symp. Pure Mathematics*, pp. 297–325. Providence, RI: American Mathematical Society.

Biktashev, V. N. & Holden. A. V. 1998 Deterministic Brownian motion in the hypermeander of spiral waves. *Physica* D **116**, 342–382.

Brahona, M. & Poon, C.-S. 1996 Detection of nonlinear dynamics in short, noisy time series. *Nature* **381**, 215–217.

Cazelles, B. & Ferriere, R. H. 1992 How predictable is chaos? *Nature* **355**, 25–26.

Coullet, P. & Emilsson, K. 1996 Chaotically induced defect diffusion. In *Instabilities and nonequilibrium structures. V* (ed. E. Tirapegui & W. Zeller), pp. 55–62. Dordrecht: Kluwer.

Eckmann, J.-P., Kamphorst, S. O., Ruelle, D. & Ciliberto, S. 1986 Liapunov exponents from time series. *Phys. Rev.* A **34**, 4971–4979.

Field, M., Melbourne, I. & Török, A. 2003 Decay of correlations, central limit theorems and approximation by Brownian motion for compact Lie group extensions. *Ergod. Theory Dynam. Syst.* **23**, 87–110.

Guckenheimer, J. & Holmes, P. 1990 *Nonlinear oscillations, dynamical systems, and bifurcations of vector fields.* Applied Mathematical Science, vol. 42. Springer.

Kawahara, T. & Toh, S. 1988 Pulse interactions in an unstable dissipative–dispersive nonlinear system. *Phys. Fluids* **31**, 2103–2111.

Melbourne, I. & Nicol, M. 2003 Statistical properties of endomorphisms and compact group extensions. Preprint, University of Surrey, UK.

Melbourne, I. & Török, A. 2002 Central limit theorems and invariance principles for time-one maps of hyperbolic flows. *Commun. Math. Phys.* **229**, 57–71.

Nicol, M., Melbourne, I. & Ashwin, P. 2001 Euclidean extensions of dynamical systems. *Nonlinearity* **14**, 275–300.

Parker, T. S. & Chua, L. O. 1989 *Practical numerical algorithms for chaotic systems*. Springer.

Parlitz, U. & Lauterborn, W. 1987 Period-doubling cascades and devil's staircases of the driven van der Pol oscillator. *Phys. Rev.* A **36**, 1428–1434.

Press, W. H., Teukolsky, S. A., Vetterling, W. T. & Flannery, B. P. 1992 *Numerical recipes in C*. Cambridge University Press.

Sano, M. & Sawada, Y. 1985 Measurement of the Lyapunov spectrum from a chaotic time series. *Phys. Rev. Lett.* **55**, 1082–1085.

Takens, F. 1981 *Detecting strange attractors in turbulence*. Lecture Notes in Mathematics, vol. 898, pp. 366–381. Springer.

van der Pol, B. 1927 Forced oscillations in a circuit with nonlinear resistance (receptance with reactive triode). *Phil. Mag.* **43**, 700.

Wolf, A., Swift, J. B., Swinney, H. L. & Vastano, J. A. 1985 Determining Lyapunov exponents from a time series. *Physica* D **16**, 285–317.